Advances in Applied Mathematics and Mechanics
Adv. Appl. Math. Mech., Vol. **5**, No. 5, pp. 607-638

DOI: 10.4208/aamm.12-m1256
October 2013

Analysis of Two-Phase Cavitating Flow with Two-Fluid Model Using Integrated Boltzmann Equations

Shuhong Liu[1], Yulin Wu[1], Yu Xu[2] and Hua-Shu Dou[3,*]

[1] *State Key Laboratory of Hydro Science and Hydraulic Engineering, Tsinghua University, Beijing 100084, China*

[2] *Institute of Engineering Thermophysics, Chinese Academy of Sciences, Beijing 100080, China*

[3] *Faculty of Mechanical Engineering and Automation, Zhejiang Sci-Tech University, Hangzhou 310018, Zhejiang, China*

Received 16 April 2012; Accepted (in revised version) 7 March 2013

Available online 31 July 2013

Abstract. In the present work, both computational and experimental methods are employed to study the two-phase flow occurring in a model pump sump. The two-fluid model of the two-phase flow has been applied to the simulation of the three-dimensional cavitating flow. The governing equations of the two-phase cavitating flow are derived from the kinetic theory based on the Boltzmann equation. The isotropic RNG $k-\epsilon-k_{ca}$ turbulence model of two-phase flows in the form of cavity number instead of the form of cavity phase volume fraction is developed. The RNG $k-\epsilon-k_{ca}$ turbulence model, that is the RNG $k-\epsilon$ turbulence model for the liquid phase combined with the k_{ca} model for the cavity phase, is employed to close the governing turbulent equations of the two-phase flow. The computation of the cavitating flow through a model pump sump has been carried out with this model in three-dimensional spaces. The calculated results have been compared with the data of the PIV experiment. Good qualitative agreement has been achieved which exhibits the reliability of the numerical simulation model.

AMS subject classifications: 76T10, 76M12

Key words: Cavitating flow, two-fluid model, RNG $k-\epsilon-k_{ca}$ turbulence model, Boltzmann equations, kinetic theory.

*Corresponding author.
Email: wyl-dhh@tsinghua.edu.cn (Y. L. Wu), huashudou@yahoo.com (H. S. Dou)

1 Introduction

Cavitating flow is a type of two-phase flow with liquid phase and vapor phase. In some cases, cavitating flow is turbulent, highly dynamic and highly unstable. There is not only momentum transfer between the liquid phase and cavity phase, but also mass transfer, that is, the vaporizing process and the liquidizing process. Because of these mentioned complexties, there are many difficulties in the numerical simulation of cavitating flow compared to the normal silt-liquid and particulate-gas two-phase flow simulation.

In recent years, there has been much progress in cavitating flow simulation. Simulation methods have been developed from inviscid flow calculation to viscous flow calculation, from two-dimensional computation to three-dimensional computation, and from single-phase flow simulation to two-phase flow simulation.

Beginning in the 1960s and 1970s, many cavitating flow models have been established based on the ideal fluid assumption and the singularity method. Yamaguchi and Kato [1] proposed a cavitating flow model, which was used widely in calculation. Brewer and Kinnas [2] used this model to calculate the flow around two-dimensional (2D) and three-dimensional (3D) hydrofoils, and Pellone and Peallat [3] used it to predict the local bubbles near the hydrofoil surface. De Lange and De Bruin [4] numerically simulated the periodic variation of bubbles.

As turbulent flow simulation has developed, it has been extended to the analysis of cavitating flow. Up to now, the most widely used method for this cavitating flow analysis is the single-phase flow model, even though the cavitating flow is actually a two-phase flow consisting of a cavity phase and a liquid phase. This single-phase cavitating flow model numerically models the flow through direct computation of the single-phase Navier-Stokes equations. A possible simplification of this type of complex flow is to assume the gas-liquid flow is a virtual single-phase, with a sharp density change as long as the pressure drops below some critical pressure (Kubota et al. [5]; Song et al. [6]).

The single-phase cavitating flow model is mainly used in fixed bubble flow calculation because the position of a fixed bubble is rather stable from the point view of direct observation. Actually, the time averaged results with this method is rather stable. The bubbles in the flow have variations in their shape, size and length over time. The liquid flow around bubbles is the main flow area, with much greater velocity than that of vapor in bubbles. Thus, in the model, the surfaces of bubbles can be assumed to be solid walls, on which the pressure is equal to the vaporizing pressure at a certain temperature.

In the single-phase simulation, the algorithm first simulates the whole flow field without bubbles; and then judges areas with pressure less than the vaporizing pressure; third, treats these areas as bubble areas; and finally, recalculates the whole flow field again. This procedure is repeated until the iteration is converged.

The single-phase simulation for cavitating flow is simple and easy, because the single turbulent simulation model and numerical method have been well developed nowadays. But its application is limited to fixed-bubble cavitating flow. For other types of cavitating flow, for example, dissociative bubble flow and bubble cloud, it may be difficult to

achieve an accurate simulation, because the single-phase calculation ignores the momentum and mass transfer between bubbles and the liquid.

It should be noted that some attractive results were obtained through a barotropic model (Arndt et al. [7]; Qin et al. [8]) to capture the main physics of complex cavitation wake flows. The simulation methodology was based on large eddy simulation (LES), using a barotropic phase model to couple the continuity and momentum equations.

The cavitating flow is actually a two-phase (cavity-liquid) flow, in which there exists mass and momentum transfer between the liquid phase and cavity phase. In contrast with the single-phase flow, there is a continuous phase (liquid phase) as well as a dispersed phase (cavity phase) in a cavitating flow. The cavities are distributed in the liquid flow in the form of dispersion.

The calculation of the two-phase flow requires simulation of both the continuous phase and the dispersed phase. According to the different simulating models of each phase, two-phase simulation models have different schemes with different combinations of each phase model. Unlike the single-phase model, the two-phase simulation should consider interaction and the mass and momentum transfers between the continuous and the dispersed phases, as well as the mass and momentum properties' jumps on the interfaces between the two phases. In two-phase simulation, the numbers of physical variables for describing the two-phase flow are doubled comparing with that for single-phase flow. For these reasons, two-phase flow simulation is much more complex (Chen and Heister [9], Deshpande et al. [10]).

For the two-phase simulation, two models can be chosen: the two-fluid model and the mixture model.

In the mixture model, it is assumed that there is a dynamic balance in both the liquid phase and cavity phase in the cavitating flow. The mixture model eliminates the difficult mutual interaction forces of the two-fluid model by summing up the momentum equations. The "lost information" is substituted via a slip relation, usually in the form of an algebraic equation. The mixture density is a function of position and time as the vapor fraction is a function of space and time. Moreover, the individual phase still has its own "density".

Chen and Heister [9] simulated the cavitating flow around an axis-symmetrical body by using the Marker and Cell method. Ventikos and Tzabiras [11] calculated the cavitation of flow around a hydrofoil and considered the temperature variation in the flow by the pressure correction method. However, these two calculations did not include the effect of turbulence in cavitating flow.

Other researchers simulated turbulent cavitating flow using N-S equations and an additional equation of the cavity (or liquid) volume (or mass) fraction. Singhal et al. [12] and Merkle et al. [13] used the mass fraction equation and $k-\varepsilon$ turbulence model to simulate a cavitating flow around a foil. Kunz et al. [14] and Brewer and Kinnas [2] used a multiple species approach with additional establishment of a mass transfer law between liquid and vapor in their relevant works. This model can be applied to the cases in which the relative motion between phases should be taken into account. Senocak

and Shyy [15] used the mass fraction equation and the $k-\varepsilon$ turbulence model, as well as the pseudo-compressibility method to simulate the three-dimensional (3D) and axis-symmetrical cavitating flows.

In the mixture model, the governing equations include the continuity and the momentum equations for the mixture, the continuity equation for the cavity as well the volume fraction equation of the cavity for the purpose of simulating the mixture of the cavitating flow.

In the two-fluid model, the dispersed phase is treated as a pseudo-fluid. In the Eulerian approach, the flow of the dispersed phase is described by the conservation equations of the mass, momentum and energy in continuous mechanics. This model includes not only the slip of parameters between the carrier fluid and the dispersed phase, but also reflects the differences in the diffusion for the carrier fluid and the dispersed phase. For example, the diffusion of the cavity phase is different from liquid diffusion. Therefore, the two fluid model can contain more information on the turbulent flow transport in two-phase cavitating flow. Rieger [16] first introduced the two-fluid model for cavitating flow simulation. Grogger and Alajbegovic [17] introduced the calculation for a cavitating flow in a Venturi tube. The disadvantages for this model are that the computation takes more time to get convergence and the iteration procedure is not stable.

In the two-fluid model, the "single-pressure" description for the continuous phase is widely used in computation, which fails to account for the cavity rebounding effect by walls and cavity collision with each other. In order to involve these effects in the frame of the two-fluid model the dispersed phase pressure and the internal transport should be considered to the dispersed phase with the dense volumetric fraction based on the kinetic theory of heterogeneous media. The problems arisen in the implementation of the two-fluid model proposes challenge to the investigators to develop two-stage discrete approaches.

In the cavitating flow, the volumetric fraction of the cavity phase varies extensively with the space and the time. In most area of the flow field, the fraction is very low, but at the cavitation area, it is high. Thus, it is necessary to use the two-fluid model to analyze the cavitating flow in the whole flow field in order to predict the behaviour of the flow field. On the bases of the theory of the two-fluids model for multiphase flows, the cavity phase, which can be assumed to be a pseudo-fluid, occupies a certain fraction volume in the whole flow domain shared with the continuum phase.

In this study, the three-dimensional cavity-liquid two-phase turbulent flows through a model pump sump are simulated under the frame of the two-fluid model. In the cavity phase, the RNG $k-\varepsilon-k_{ca}$ turbulence model is employed, while the RNG $k-\varepsilon$ turbulent model is used in the liquid phase. The program is developed in the non-orthogonal body-fitted coordinate (BFC) system for three-dimensional spaces. The governing equations of the two-phase cavitating flow have been deduced from the kinetic theory based on the Boltzmann equation. The calculated results have been compared with a PIV experiment. Good agreement exhibits the reliability of the present model and the present numerical simulation.

2 Governing equations of cavitating two-phase flow in two-fluid model

Several researchers have obtained the governing equations of the cavitating flow in terms of the macroscopic continuous mechanics theory. As the fluid vaporizes (gasificates) if the local pressure in the flow is lower than the vapor pressure of the fluid, and the gas quickly condensates if the pressure is higher than vapor pressure, the diameters of the cavity vary with the local pressure, which results in the mass and momentum transfers. These can hardly be described by the governing equations from macroscopic model. For this reason, other models based on the microscopic kinetic theory should be introduced.

The derivation of the governing equations of dense particle-liquid two-phase flows was briefly discussed by Tang and Wu [18]. In the present work, based on Boltzmann equation, governing equations for two-phase cavitating flow are developed, in which the terms in the equations for mass and momentum transfers can be obtained. The feature in this study is that the cavity number is employed instead of the cavity phase volume fraction. The advantage of the present formulations is that it can predict the variations of both the cavity diameter and the cavity number in a unit volume. In such a way, the model developed in the present study can predict the cavitation clouds.

The starting point is the microscopic Boltzmann equation. By weighting the Boltzmann equation of each phase by property parameters and integrating over the velocity space, the continuity and momentum equations are derived. The derivation details and glossary of symbols are discussed in Appendix. The results are summarized here.

Let α_l and α_{ca} be the volume fractions of the liquid and cavity phases respectively, and $\alpha_{ca}+\alpha_l=1$. The governing equations (continuity and the momentum equations) for the liquid-phase are (see Appendix A and B),

$$\frac{\partial \alpha_l \rho_l}{\partial t}+\frac{\partial}{\partial x_j}(\alpha_l \rho_l \mathbf{u}_{lj})=S_l, \tag{2.1a}$$

$$\frac{\partial(\alpha_l \rho_l \mathbf{u}_{li})}{\partial t}+\frac{\partial}{\partial x_j}(\alpha_l \rho_l \mathbf{u}_{li}\mathbf{u}_{lj})=\alpha_l \rho_l g_{li}-\frac{\partial(\alpha_l p)}{\partial x_i}+\alpha_l \frac{\partial \tau_{lij}}{\partial x_j} + \frac{\alpha_l \rho_l}{\tau_{rca}}(\mathbf{u}_{cai}-\mathbf{u}_{li})+\mathbf{u}_{li}S_l, \tag{2.1b}$$

where $\mathbf{u}$ is the mean velocity in the liquid phase or cavity phase from a macroscopic view. And

$$S_{ca}=-S_l=(n4\pi)^{\frac{1}{3}}(3\alpha_{ca})^{\frac{2}{3}}\frac{\rho_{ca}\rho_l}{\rho}\left[\frac{2}{3}\left(\frac{p_v-p}{\rho_l}\right)\right]^{\frac{1}{2}}, \tag{2.2a}$$

$$\rho=\alpha_{ca}\rho_{ca}+\alpha_l\rho_l, \quad \tau_{rca}=\frac{d_{ca}^2\rho_{ca}}{18\mu_l}\left(1+\frac{Re_{ca}^{\frac{2}{3}}}{6}\right)^{-1}, \quad Re_{ca}=\left|\mathbf{u}_{ca}-\mathbf{u}_l\right|\frac{d_{ca}}{\nu_l}. \tag{2.2b}$$

The governing equations for the cavity-phase are

$$\frac{\partial \alpha_{ca}\rho_{ca}}{\partial t}+\frac{\partial}{\partial x_j}(\alpha_{ca}\rho_{ca}\mathbf{u}_{caj})=S_{ca}, \tag{2.3a}$$

$$\frac{\partial(\alpha_{ca}\rho_{ca}\mathbf{u}_{cai})}{\partial t}+\frac{\partial}{\partial x_j}(\alpha_{ca}\rho_{ca}\mathbf{u}_{cai}\mathbf{u}_{caj})=\alpha_{ca}\rho_{ca}g_{cai}-\frac{\partial(\alpha_{ca}p)}{\partial x_i}+\frac{\alpha_{ca}\rho_{ca}}{\tau_{rca}}(\mathbf{u}_{li}-\mathbf{u}_{cai})+\mathbf{u}_{cai}S_{ca}. \tag{2.3b}$$

3 RNG $k-\varepsilon-k_{ca}$ turbulence model of cavitating two-phase turbulent flow

In the present work, the RNG $k-\varepsilon-k_{ca}$ turbulence model, that is RNG $k-\varepsilon$ model in the liquid phase and k_{ca} model in the cavity phase, is used to close the equations.

The k and ε equations of the RNG $k-\varepsilon$ model for liquid phase are as follows:

$$\rho_l\frac{\mathrm{D}k}{\mathrm{D}t}=\frac{\partial}{\partial x_j}\Big(\sigma_k\mu_{eff}\frac{\partial k}{\partial x_j}\Big)+G_k+G_p+G_R-\rho_l\varepsilon, \tag{3.1a}$$

$$\rho_l\frac{\mathrm{D}\varepsilon}{\mathrm{D}t}=\frac{\partial}{\partial x_j}\Big(\sigma_\varepsilon\mu_{eff}\frac{\partial \varepsilon}{\partial x_j}\Big)+\frac{\varepsilon}{k}\big[C_{\varepsilon1}(G_k+G_p)-C_{\varepsilon2}\rho_l\varepsilon\big]-R, \tag{3.1b}$$

$$G_k=\mu_t\Big(\frac{\partial \mathbf{u}_{li}}{\partial x_j}+\frac{\partial \mathbf{u}_{lj}}{\partial x_i}\Big)\frac{\partial \mathbf{u}_{li}}{\partial x_j},\quad G_p=-\frac{\alpha_{ca}\rho_{ca}}{\tau_{rp}}\big[2(k-C_p^k\sqrt{kk_{ca}})\big],\quad G_R=2kD, \tag{3.1c}$$

where

$$D=(2D_{ij}D_{ij})^{\frac{1}{2}}\quad\text{and}\quad D_{ij}=\frac{1}{2}\Big(\frac{\partial \mathbf{u}_{lj}}{\partial x_i}+\frac{\partial \mathbf{u}_{li}}{\partial x_j}\Big).$$

The effective viscosity can be obtained from this formula:

$$d\Big(\frac{\rho k^2}{\sqrt{\varepsilon\mu}}\Big)=1.72\frac{\hat{\mu}}{\sqrt{\hat{\mu}^3-1+C_V}}d\hat{\mu}, \tag{3.2}$$

where $\hat{\mu}=\mu_{eff}/\mu$ and $C_V\approx100$

$$R=\frac{C_\mu\rho\eta^3(1-\eta/\eta_o)}{1+\beta\eta^3}\frac{\varepsilon^2}{k},$$

where

$$\eta=D\frac{k}{\varepsilon},\quad \eta_o=4.38,\quad C_\mu=0.0845,\quad \beta=0.012,$$
$$C_{\varepsilon1}=1.42,\quad C_{\varepsilon2}=1.68,\quad \sigma_k=1.0,\quad \sigma_\varepsilon=0.769.$$

And the k equation in the k_{ca} turbulence model for cavity phase is:

$$\frac{\partial}{\partial t}(\alpha_{ca}k_{ca})+\frac{\partial}{\partial x_j}(\alpha_{ca}\mathbf{u}_{caj}k_{ca})=\frac{\partial}{\partial x_j}\left(\alpha_{ca}\frac{\nu_{ca}}{\sigma_p}\cdot\frac{\partial k_{ca}}{\partial x_j}\right)+G_{kca}+G_{pca}-\alpha_{ca}\varepsilon_{ca}, \tag{3.3a}$$

$$G_{kca}=\alpha_{ca}\nu_{ca}\left(\frac{\partial \mathbf{u}_{caj}}{\partial x_j}+\frac{\partial \mathbf{u}_{cai}}{\partial x_j}\right)\frac{\partial \mathbf{u}_{cai}}{\partial x_j},\quad G_{pca}=\frac{\nu_{ca}}{\sigma_p}\left(\frac{\partial \alpha_{ca}}{\partial x_i}\cdot\frac{\partial \mathbf{u}_{cai}}{\partial x_j}\right), \tag{3.3b}$$

$$\varepsilon_{ca}=-\frac{1}{\tau_{rca}}\left[2(C_p^k\sqrt{kk_{ca}}-k_{ca})+\frac{\mathbf{u}_{cai}}{\alpha_{ca}}\cdot\frac{\nu_{ca}}{\sigma_p}\cdot\frac{\partial \alpha_{ca}}{\partial x_i}\right], \tag{3.3c}$$

where $\sigma_p=1.5$, $C_p^k=0.11$.

In the numerical procedure, one of the SIMPLE algorithms, named as SIMPLEC, is used to solve the equations in both liquid and cavity phases.

4 Numerical procedure of the simulation

4.1 Computational domain and parameters of the model pump sump

Pump sumps are widely used in various installations like cooling water systems. Modern industrial devices require demand of pump sumps of very large capacities with good performances. The flow conditions in the pump suction sump are very complicated, especially, in the surrounding of the pump bell (Fig. 1), where there are various types of vortexes and in some cases these vortexes induce cavitation, which result in vibration. These effects reduce the performance of the pump station and may result in the breakdown of the device.

The 3D cavitating two-phase turbulent flow calculations are based on a closed pump sump, for which the experimental data is available. The configuration of the test pump sump is shown in Fig. 1. The main section is divided into two identical channels (A and B) vertically by clapboard. The pipe bell with special structure is manufactured using Plexiglas material. The experimental data are obtained by PIV technology.

The flow rates in two channels are $0.965m^3/min$ (A) and $0.64m^3/min$ (B) respectively. In the calculation, the whole flow area is modeled in computation, and some represen-

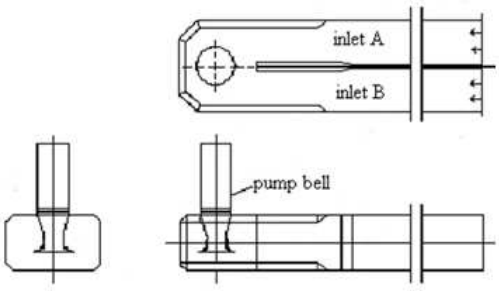

Figure 1: Pump sump model configuration.

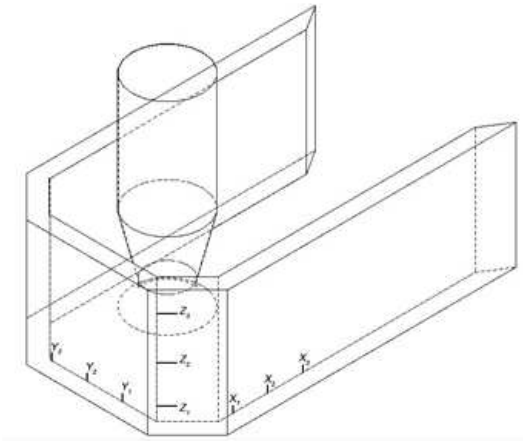

Figure 2: Positions of measuring planes.

tative planes are chosen here to show the results. The sketch of measurement planes is shown in Fig. 2 and Table 1.

Here, Planes X_2, Y_1 and Y_3 are tangent with the bell edge; Plane X_1 is near the back wall; Planes X_3 and Y_2 are on the center of pipe bell; Planes Z_1, Z_2 and Z_3 are below, tangent with and above the bell inlet.

With the method described above, the computation of three-dimensional two-phase cavitating flow through a model pump sump has been carried out. Simulation results are shown below, and are compared with a PIV experiment.

Table 1: The parameters of water and vapor at the inlet of the pump sump test.

	temperature	Density (kg/m^3)	Viscosity $(Pa\times s)$	vaporizing pressure (kPa)	volume fraction at inlet
Water	20° C	0.998203	1.0087×10^{-3}		
Vapour	20° C	0.017313	9.669×10^{-6}	2.3388	10^{-5}

4.2 Numerical treatments

The governing equations are discretized in the Cartesian coordinates using the finite volume method with structured hexahedral and unstructured tetrahedral meshes. The second order central difference scheme is used to discretize the diffusion term and the second order upstream difference is used to discretize the convective term. Finally, the discretization of the governing equations in the whole domain forms a system of algebraic equations at each time step.

In the present computation, the iterative procedure between the liquid phase flow and the cavity flow is necessary based on each phase flow computation. In order to get the convergent solution of the two phase flows, the interaction between the two phases should be considered. In the procedure, the calculation algorithm of liquid phase is the

same as that for single phase flow computation. By using one of the SIMPLE algorithms or the SIMPLEC, one can get the solution of the velocity field and the pressure field of the liquid phase. Then the solver for the cavity phase will start based on the first solution of liquid phase and the initial condition of the cavity phase. In the cavity computation, the volumetric fraction of cavity will be obtained through solving the continuous equation and the Rayleigh equation, and at the same time, the velocity of cavity will be solved out through the numerical solution of the momentum equation. Then the convergent solution for the cavity phase will be achieved after the interactive computation for each phase. In the solution, the velocity of cavity flow is much lower comparing with the liquid velocity. The volumetric fraction of cavity phase is one of the main results of the solution of cavity phase.

In the computation, the maximum error in satisfying the momentum equations at convergence was smaller than 10^{-5} and, the maximum error in satisfying the continuity equation was of the order of 10^{-4}. These are in the range expected of a second-order method with proper grid spacing. That is to say, the computation does not have a large error. The experimental uncertainty is about 5% to 10%. The large difference at the peak value of the velocity components is mainly induced by the turbulence model. The $k-\varepsilon$ turbulence model can not simulate large eddy in fluid flow, which usual occurs in cavitating flows.

The computational solved domain is shown as in Fig. 1. The domain's grids are composed of unstructured hexahedron elements. In order to make y+ small enough to 40-50, wall of the outlet pipe boundary has 4 layers and there are local refinements on both sides of the outlet pipe in the sump. The total mesh numbers of the domain are 2364746. The initial conditions of inlet velocity components and static pressures at inlet branches were given according to the test data.

4.3 Boundary conditions

- Inlet condition: The first type of boundary conditions is given at the inlet.
- Outlet condition: The derivatives of velocity components $\mathbf{u}_j$ and k, ε are zero along the normal of the boundaries, that is,

$$\frac{\partial \mathbf{u}_j}{\partial n}=0, \quad (j=1,2,3), \quad \frac{\partial k}{\partial n}=0, \quad \frac{\partial \varepsilon}{\partial n}=0. \tag{4.1}$$

- Wall conditions: Near solid walls, the logarithmic velocity profile was used to calculate the velocity and k, ε. Supposing that the distance from the nearest station P to the wall is y_p, then the values of $\mathbf{u}_p$, k_p, ε_p can be defined as:

$$\frac{\mathbf{u}_p}{\mathbf{u}_\tau}=\frac{1}{\kappa}\ln(Ey_p^+), \quad k_p=\frac{u_\tau^2}{\sqrt{C_\mu}}, \quad \varepsilon_p=\frac{u_\tau^3}{\kappa y_p}, \tag{4.2}$$

where

$$y_p^+ = \frac{\rho \mathbf{u}_\tau y_p}{\mu} = \frac{\rho c_\mu^{\frac{1}{4}} k_p^{\frac{1}{2}} y_p}{\mu}, \quad \mu_\tau = \sqrt{\frac{\tau_w}{\rho_f}}. \tag{4.3}$$

- Pressure conditions: The normal derivatives of pressure on all boundaries is zero. And the inlet pressure which was obtained through experiment is given as the reference pressure.

The inlet conditions of velocity and volumetric fraction are given according to the liquid phase. Outlet condition and the wall condition is the second type, and the derivatives along the normal to boundaries are zero

$$\frac{\partial v_i}{\partial n}\Big|_{y=0} = 0, \quad (i = 1,2,3). \tag{4.4}$$

5 Experimental description

The pump suction sump and pump bell used in the experiments are different from the general ones.

5.1 Experimental system

The main component of the laboratory model is an approximately rectangular pump sump. The configuration of the pump sump model is shown in Fig. 1, and the positions of measuring planes are shown in Fig. 2. The structure of the pump suction sump is sketched in Fig. 3. The inlet of the sump is divided vertically into two identical channels by the clapboard, which has a special requirement on size. From the view of the inlet, inlet A is on the left side and inlet B is on the right side. The purpose of using two inlets is to allow the creation of asymmetric flow surrounding the pump bell, which makes the experimental set-up more general, and allows simulation of more typical conditions. Trash

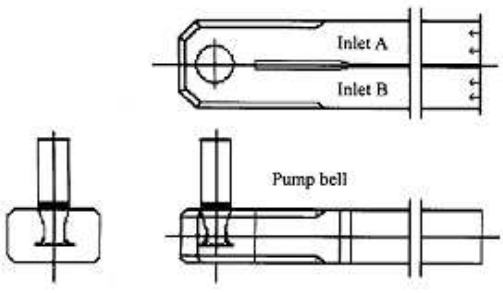

Figure 3: Structure of the pump suction sump.

racks are placed in front of each inlet to stabilize the flow. The verges of the pump suction sump near the bell are designed with a smooth shape to optimize the flow conditions.

The pump bell in this experiment was manufactured on a numerically controlled lathe using organic glass material. The inlet of the pump bell is also specially designed to optimize the flow in the pipe. The pump bell connects with the upper wall of the pump sump. On the top of the bell, there is a vertical pipe, and the water is pumped through it upwards from the bell.

5.2 PIV system arrangement

The PIV system, purchased from TSI Inc., consists of a two 2-pulsed Nd:Yag laser, a CCD camera, a synchronizer, and a data analysis system. The output power of the laser is $120mJ/Puls$, which is sufficiently high for the experiment. The interval of the second exposure was longer than that of the first. The interval of the two pulses was chosen according to the velocity values. The lower the measured velocity, the larger the interval used. The CCD camera was used to obtain digital images with 1300×1000 pixels, and can capture 3. 75 images in one second. The particles used in these experiments are hollow glass particles with diameters of $10\sim20\mu m$. Fig. 4 shows a sketch of the PIV system arrangement in the measurement.

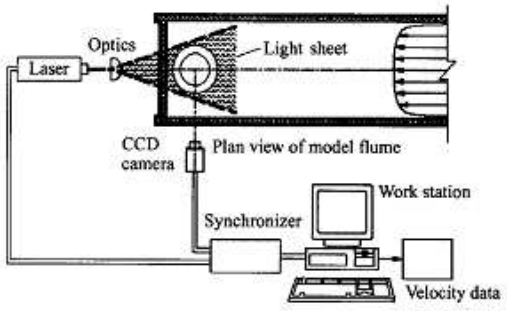

Figure 4: PIV system arrangement in the measurement.

5.3 PIV measurement uncertainty

In general, the uncertainty in the mean velocity components in the channel measured by ADV was estimated to be about 6%. The LDV system measured the turbulence intensity in the streamwise direction within 1%. The uncertainty in the instantaneous velocities measured by PIV was estimated at 5% of the maximum velocity.

We have made detailed measurement to determine the uncertainty in the measurement of velocity in a channel, as shown in Fig. 5. This figure indicates the velocity component on the measuring plane at two sampling points. PIV measurement uncertainty of

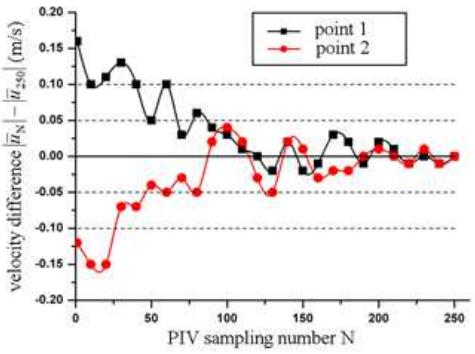

Figure 5: Measuring uncertainty at speed variation condition.

velocity is defined as follows:

$$y=|\bar{\mathbf{u}}_N|-|\bar{\mathbf{u}}_{250}|=\frac{1}{N}\sum_{i=1}^{N}\mathbf{u}_i-\frac{1}{250}\sum_{i=1}^{250}\mathbf{u}_i,$$

where $\mathbf{u}_i$ is velocity sample at i time of measurement. N is sampling number. $N_{\max}=250$ in this experiment.

It can be seen from Fig. 5 that if the times of measurement are larger than 200, the uncertainty of measuring velocity is less than $\pm 0.03 m/s$, i.e., the error of this velocity measurement is less than $\pm 4\%$.

6 Comparisons of simulation results with experiments

In this study, simulation results on certain planes of the model pump sump are compared with the experimental results. From the numerical simulation and the PIV experiment, flow characters can be obtained respectively. The parameters of water and vapor at the inlet of the pump sump test are shown in Table 2. Comparisons of the simulation results with experiments are as follows.

Table 2: Detailed positions of measuring planes.

Planes	Positions	Coordinates
X_1	Near the back wall	$x=40mm$
X_2	Tangent with bell edge	$x=120mm$
X_3	Center of pipe	$x=200mm$
Y_1	Tangent with bell edge	$y=40mm$
Y_2	Center of pipe	$y=120mm$
Y_3	Tangent with bell edge	$y=200mm$
Z_1	Below the bell inlet	$z=50mm$
Z_2	Tangent with bell inlet	$z=80mm$
Z_3	Above the bell inlet	$z=120mm$

Figs. 6 to 14 show the comparisons of the two dimensional velocity distributions on planes Y_1, Y_2 and Y_3 (parallel to the side walls), planes of X_1, X_2 and X_3 (parallel to the back wall of the sump) and Z_1, Z_2 and Z_3 (parallel to the bottom wall) respectively, in which figures on the left side, named as (a) are experiment results, and others (b) are simulation ones. Figs. 15 to 23 show the streamlines on these planes.

Figs. 24(a) to (d) indicate the volume fraction of cavity phase on planes X_2, Y_2, Z_1 and Z_2 planes from computational results. The volume fraction of cavity is induced by the vortex cavitation on the central area of the suction pipe in the sump. In other areas in the sump there is not any cavitation occurrence to be observed in the experiment. Fig. 25 shows an experimental result of the cavity below bell inlet as an example.

Figs. 26(a) and (b) show the velocity components U and V distributions on the central line parallel to the side wall. Figs. 27(a) and (b) show the velocity components U and V distributions on the central line parallel to the back wall below the bell inlet at a distance of $50mm$ from the sump bottom surface.

For a quantitative comparison between computational results and experimental data, the difference between computational results and experimental data can be found in Figs. 26(a) to 27(b). The maximum difference is located at the peak values of the velocity components distributions. The relative maximum difference is about 19% at the peak areas. And the numerical values at these areas are a little less than the experimental data.

6.1 Velocity magnitude distribution

Figs. 6, 7 and 8 show the velocity distribution on planes Y_1, Y_2 and Y_3. Plane Y_1 is located in the channel B, and the velocity value with the maximum of $0.429m/s$ (from the experimental data) on this plane is slightly smaller than those on plane Y_3. The maximum value of velocity on plane Y_3 is $0.643m/s$, because the flow rate in channel A is 1.5 times of that

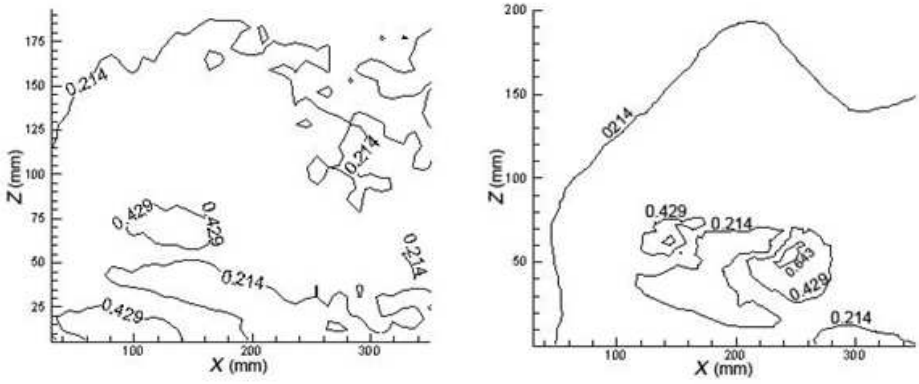

(a) Experiment (b) Simulation

Figure 6: Velocity distribution on Y_1 plane (velocity unit: m/s).

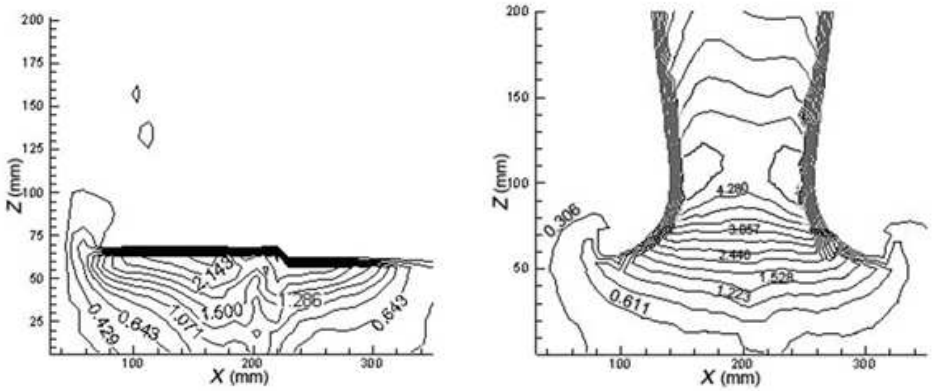

(a) Experiment (b) Simulation

Figure 7: Velocity distribution on Y_2 plane (velocity unit: m/s).

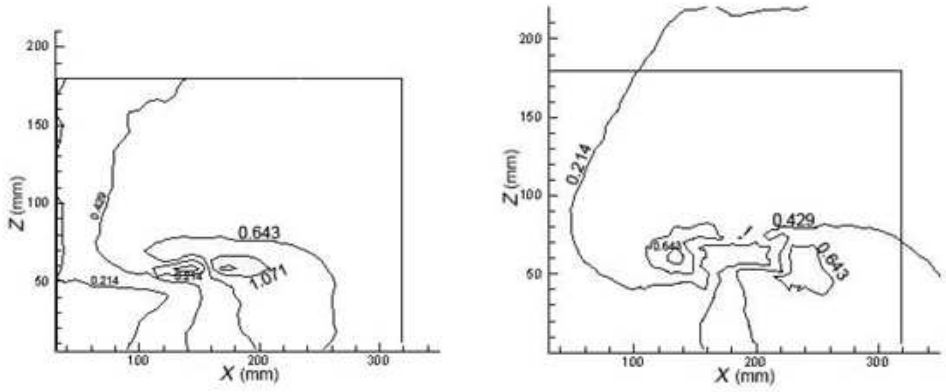

(a) Experiment (b) Simulation

Figure 8: Velocity distribution on Y_3 plane (velocity unit: m/s).

in channel B. On the central plane Y_2 in Fig. 7, the velocity values of both measured and simulated results are nearly equal below the bell inlet, which are about o.6 to $1.2m/s$. The simulated results can give the velocity distribution in the suction pipe of the pump, which show the maximum velocity on the planes is about $0.417m/s$ near the bell throat.

Velocity distribution on the central plane X_3 parallel to back wall in Fig. 11 is similar as that on the central plane Y_2 parallel to side wall in Fig. 7. Velocity distribution on plane X_1 in Fig. 9 is smaller than that on plane X_2 in Fig. 10, because this plane X_1 is close to the back wall. Both velocities from the experiment and the simulation on plane X_2 agree with each other in Fig. 10. But on plane X_1, the value from experimental results in Fig. 9(b) is smaller than that from the simulated data in Fig. 9(b).

Velocity distributions from both experiment (a) and simulation (b) on planes Z_1, Z_2 and Z_3 agree well with each other.

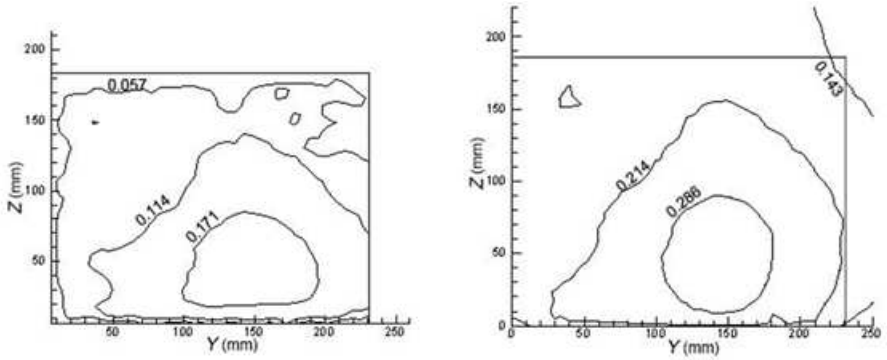

(a) Experiment (b) Simulation

Figure 9: Velocity distribution on X_1 plane (velocity unit: m/s).

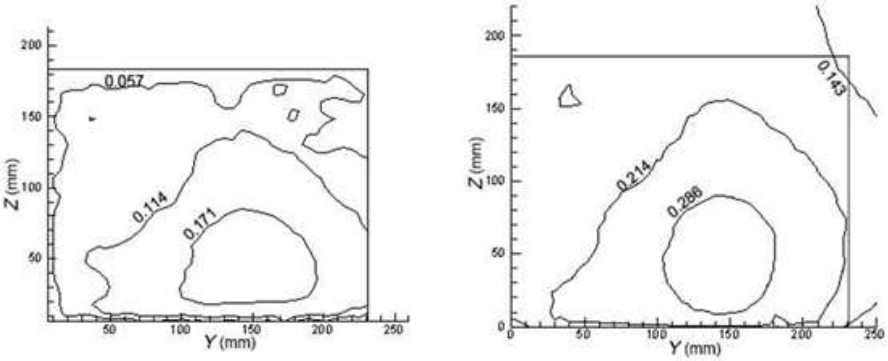

(a) Experiment (b) Simulation

Figure 10: Velocity distribution on X_2 plane (velocity unit: m/s).

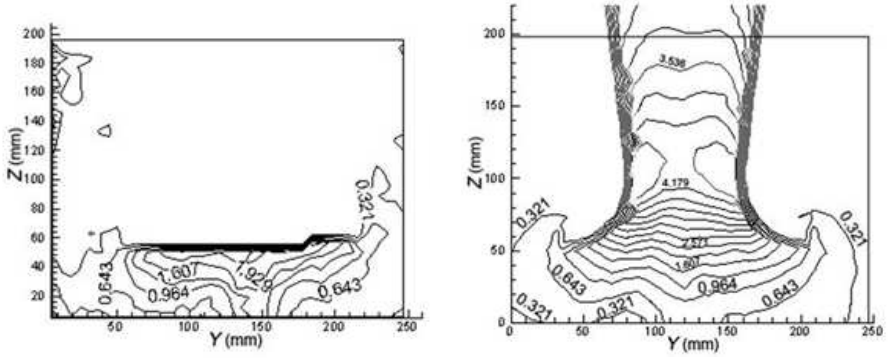

(a) Experiment (b) Simulation

Figure 11: Velocity distribution on X_3 plane (velocity unit: m/s).

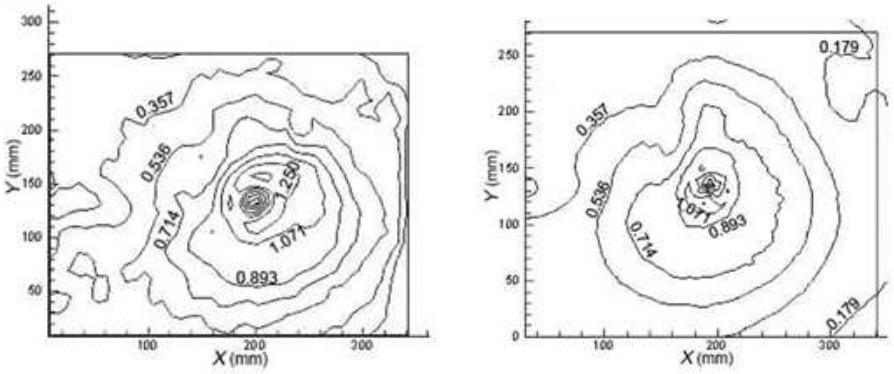

(a) Experiment (b) Simulation

Figure 12: Velocity distribution on Z_1 plane (velocity unit: m/s).

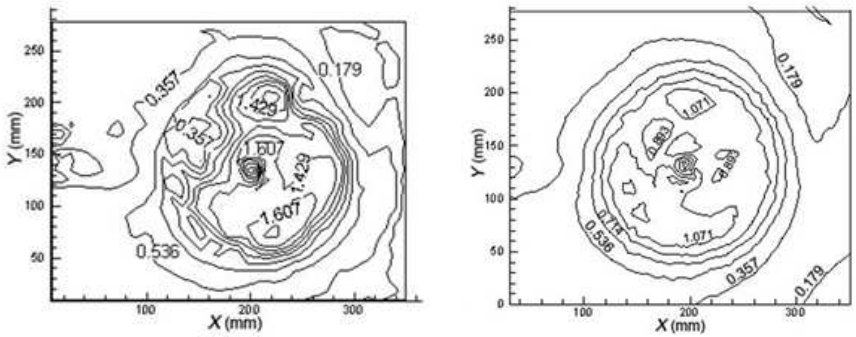

(a) Experiment (b) Simulation

Figure 13: Velocity distribution on Z_2 plane (velocity unit: m/s).

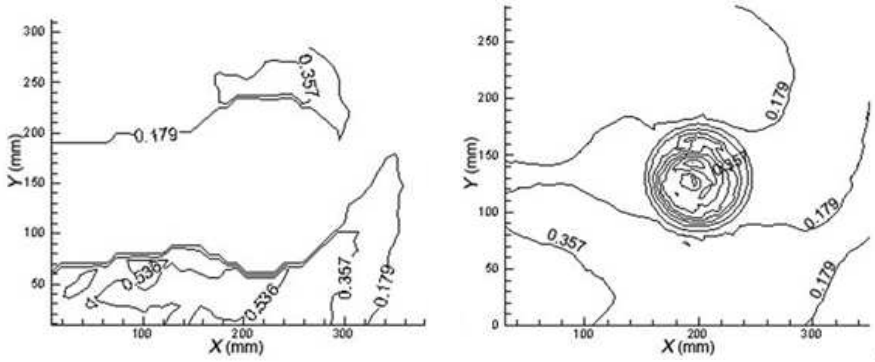

(a) Experiment (b) Simulation

Figure 14: Velocity distribution on Z_3 plane (velocity unit: m/s).

6.2 Streamline and velocity vector

Streamline distributions from both the experiment and the simulation in Fig. 15 to Fig. 23 show the similar results, which verify the validity of the simulation of velocity distributions on these planes.

Figs. 21, 22 and 23 show the streamlines on Plane z_1, z_2 and z_3. Due to the flow asymmetry at the inlet, a vortex is observed near the pipe-bell center. Since the flow rate in channel A is larger than that in channel B, it is understandable that the vortex rotates in the direction from A to B. There is another vortex observed in the corner based on the results on plane z_3 (Fig. 23). It rotates in the same direction of the center vortex.

6.3 Volume fraction of the cavity phase

Figs. 24(a) to 25 show the distribution of the volume fraction of vapor. Figs. 24(a) to (d) are the simulation results and Fig. 25 is the photo of experimental result below the bell inlet. From these figures, it can be seen that in the closed pump sump, there is a strong

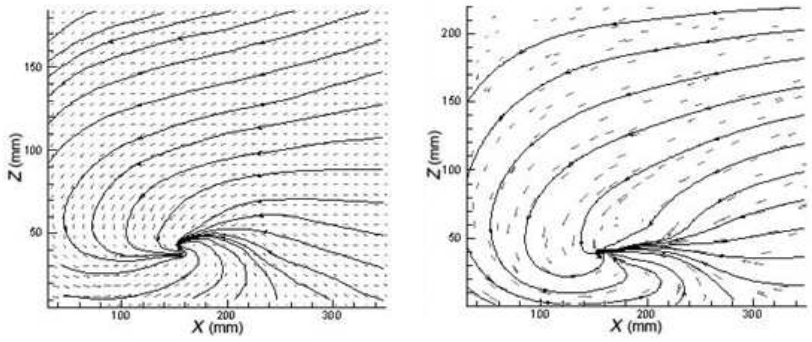

(a) Experiment (b) Simulation

Figure 15: Streamlines and velocity vectors on Y_1 plane.

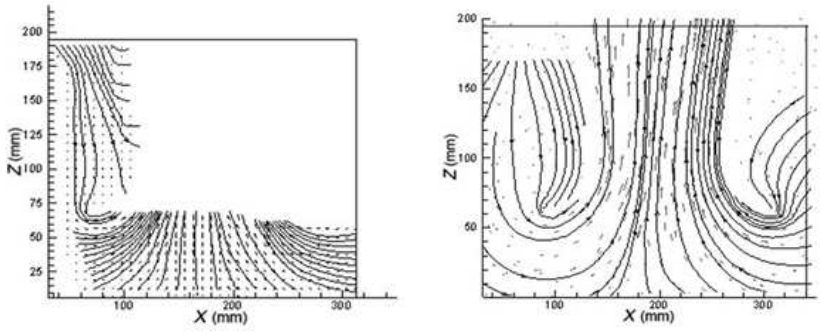

(a) Experiment (b) Simulation

Figure 16: Streamlines and velocity vectors on Y_2 plane.

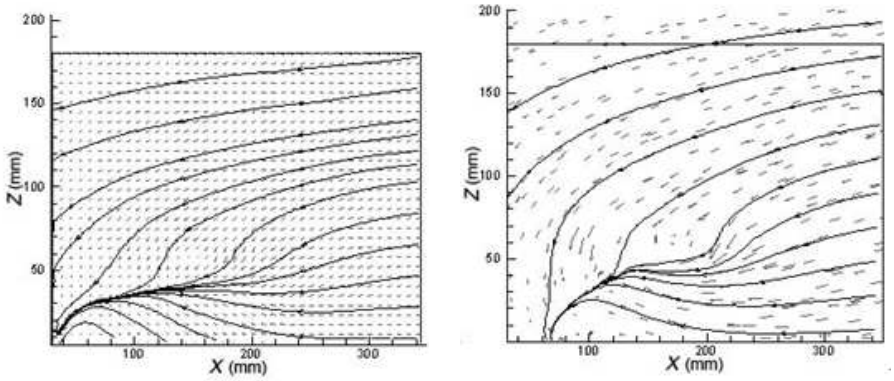

(a) Experiment (b) Simulation

Figure 17: Streamlines and velocity vectors on Y_3 plane.

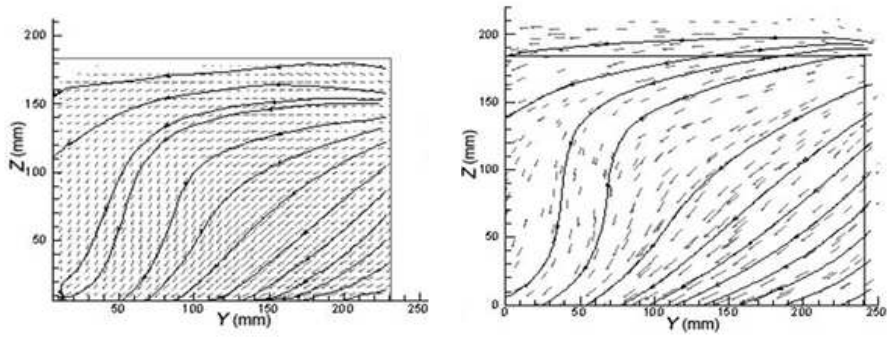

(a) Experiment (b) Simulation

Figure 18: Streamlines and velocity vectors on X_1 plane.

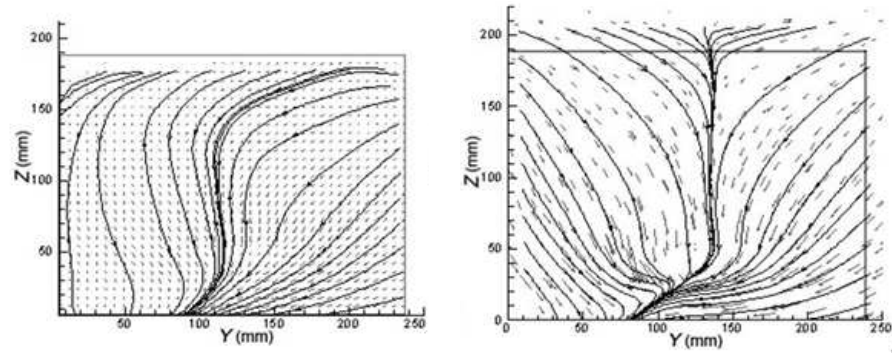

(a) Experiment (b) Simulation

Figure 19: Streamlines and velocity vectors on X_2 plane.

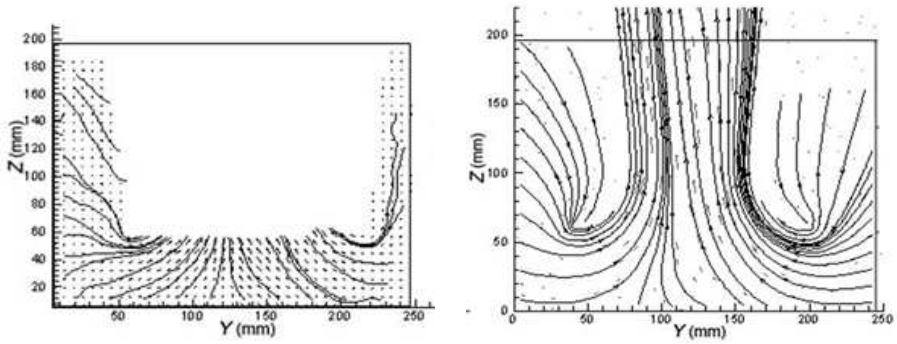

(a) Experiment (b) Simulation

Figure 20: Streamlines and velocity vectors on X_3 plane.

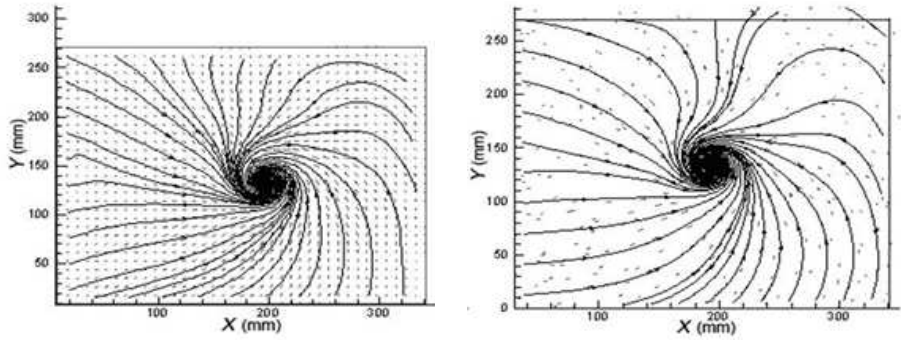

(a) Experiment (b) Simulation

Figure 21: Streamlines and velocity vectors on Z_1 plane.

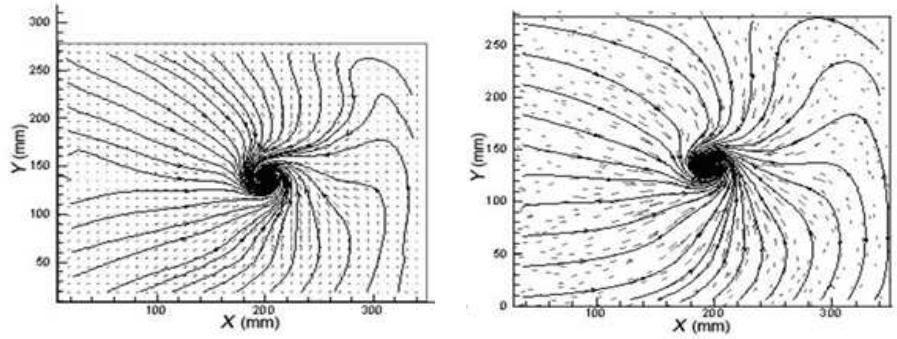

(a) Experiment (b) Simulation

Figure 22: Streamlines and velocity vectors on Z_2 plane.

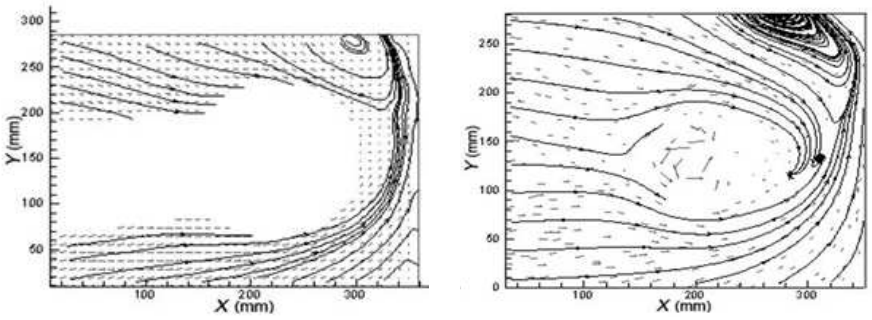

(a) Experiment (b) Simulation

Figure 23: Streamlines and velocity vectors on Z_3 plane.

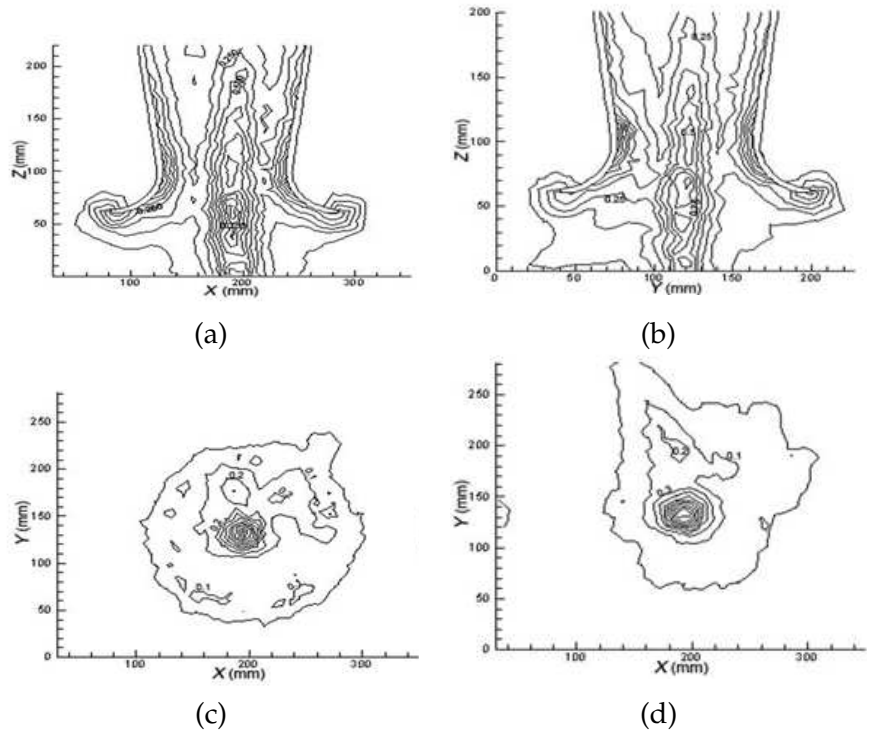

(a) (b)

(c) (d)

Figure 24: Volume fraction of cavity on (a) Y_2 plane; (b) on X_3 plane; (c) on Z_1 plane; (d) on Z_2 plane.

vortex below the bell inlet and vortex inducing cavitation occurs, which can be described by the value of the volume fraction of vapor. In this PIV experiment, limited by the experiment conditions, the volume fraction of vapor cannot be obtained and cavitation was recorded by taking photos of the position of the air core. From qualitative analysis, it can be seen that the simulation results show reasonable agreement with experimental results.

Figure 25: Experimental result of the cavity below bell inlet.

6.4 Velocity components on the central line parallel to back wall

The calculated results have been compared with a PIV experiment, and good agreement of velocity distribution on the central lines below the bell inlet has been obtained which can be observed from Fig. 26(a) to Fig. 27(b). These results exhibit the reliability of the numerical simulation model.

7 Conclusions

In the two-phase cavitating flow, the volume fraction of the cavity changes extensively in space and time. In order to capture the cavitation development in various flows, it is necessary to use the two-fluid model to analyze the complex cavitating flow. In this work, the governing equations of the two-phase cavitating flow have been developed from the kinetic theory based on the Boltzmann equation. In this cavitation model, the

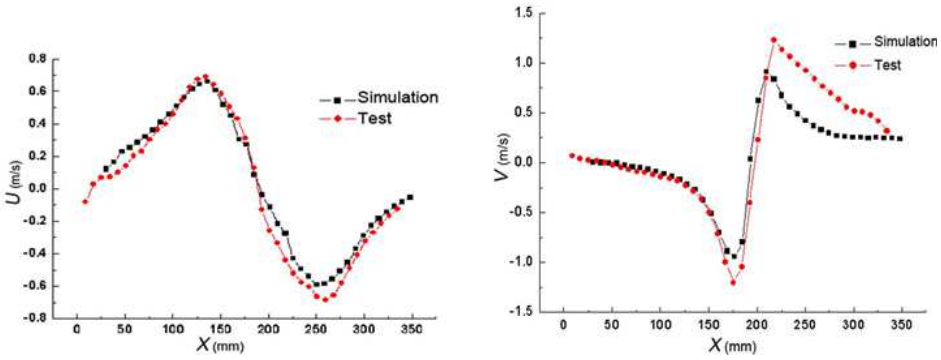

(a) (b)

Figure 26: Velocity distribution on the central line parallel to side wall on intersectional line between Z_1-Y_2 plane. (a) U; (b) V.

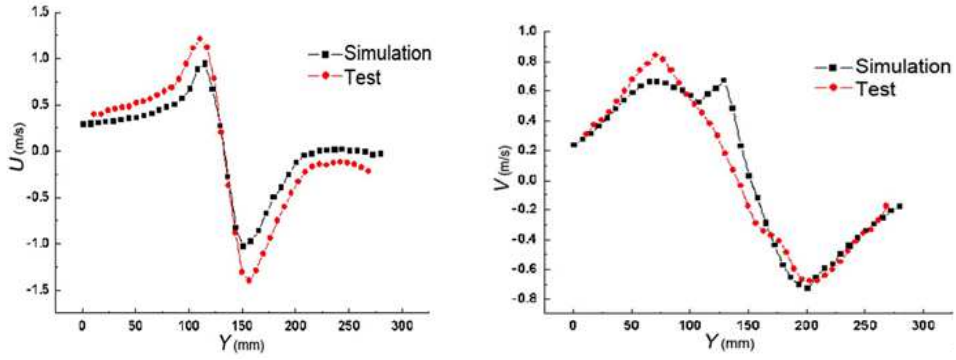

(a) (b)

Figure 27: Velocity component distribution on central line parallel to back wall on intersectional line between Z_1-X_3 plane. (a) U; (b) V.

mass transfer is obtained by considering the radius change of bubbles in cavity phase, and the interaction term is obtained by considering the interaction between the cavity and liquid. The feature of the proposed model is that the cavity number is employed instead of the cavity phase volume fraction. It can predict the variations of both the cavity diameter and the cavity number in a unit volume. In such a way, the model developed in present study can predict the cavitation clouds.

For calculating the turbulence, the RNG $k-\varepsilon-k_{ca}$ turbulence model for cavitating flow, which is the RNG $k-\varepsilon$ turbulent model for liquid phase combined with the k_{ca} model for cavity phase, is used to close the Reynolds time-averaged governing equations.

The proposed two-fluid model has been successfully used to simulate the cavitating flow in a 3D closed pump sump. After comparing the simulation results with the PIV experimental data for the 3D case, it is concluded that the present two-fluid model derived in this study is valid to reproduce all the properties of cavitations.

Appendix A: Derivation of the governining equations in two-phase flow by the Boltzmann equation

Firstly assuming that: (1) There is only translation motion and no rotation in cavity-phase; (2) The volume unit $d\mathbf{R}_k$ is much smaller than macro space, but much larger than every micro cavity volume, that is to say, it includes numerous micro cavities. Therefore, statistical approach can be applied to the cavity-phase, where $\mathbf{R}_k$ is the vector radius of micro cavity in geometric space.

A.1 Definition of variables

The molecular kinetic theory is currently used to deal with the micro cavities or particles in two-phase flow. In molecular kinetic theory, $\mathbf{c}$ is the velocity of molecules of the liquid

phase or cavity phase, $\mathbf{u}$ is the mean velocity in the liquid phase or cavity phase from a macroscopic view; that is, the mean molecule velocity, $\mathbf{c}'$, is the relative velocity of molecules to the mean macroscopic velocity, that is

$$\mathbf{c}=\mathbf{u}+\mathbf{c}' \quad \text{and} \quad \mathbf{u}=\langle\mathbf{c}\rangle, \tag{A.1}$$

where $\langle\rangle$ indicates a statistical averaged value.

In statistical mechanics, the phase space includes the radius space of molecules r, the temperature space θ, the velocity space $\mathbf{c}(x_1,x_2,x_3)$ and the geometrical space $\mathbf{R}(x_1,x_2,x_3)$ of the flow. At the time moment t, the temperature is in the $\theta\to\theta+d\theta$ range, the radius is in the $r\to r+dr$ range, the geometric position is $\mathbf{R}\to\mathbf{R}+d\mathbf{R}$, and the mean velocity of micro molecules is $\mathbf{c}\to\mathbf{c}+d\mathbf{c}$. Then, the micro molecule number at the moment is:

$$dN=f(\mathbf{R},\mathbf{c},r,\theta,t)d\mathbf{R}d\mathbf{c}d\theta dr, \tag{A.2}$$

where $d\mathbf{R}=dx_1dx_2dx_3$ indicates the volume of an element in the geometric space, $d\mathbf{c}=dc_1dc_2dc_3$ is the "volume" of an element in the velocity space, and f is the micro molecular velocity distribution function in the phase space consisting of $\mathbf{R}$ and $\mathbf{c}$. Using these, we can express the moving characteristics of a micro liquid. And any variation of the function will induce the change of macromovement characteristics of the flow. The micro molecules' number density is:

$$n=\int_{-\infty}^{+\infty}fd\mathbf{c}d\theta dr=n(\mathbf{R},\theta,r,t), \tag{A.3}$$

where Φ represents a physical variable depending upon the velocity of the micro molecules, and its statistical mean value is:

$$\langle\Phi\rangle=\frac{\int_{-\infty}^{+\infty}\Phi fd\mathbf{c}d\theta dr}{\int_{-\infty}^{+\infty}fd\mathbf{c}d\theta dr}=\frac{\int_{-\infty}^{+\infty}\Phi fd\mathbf{c}d\theta dr}{n}. \tag{A.4}$$

So the macro mean velocity of a fluid $\mathbf{u}$ is

$$\mathbf{u}=\langle\mathbf{c}\rangle=\frac{\int_{-\infty}^{+\infty}\mathbf{c}fd\mathbf{c}d\theta dr}{n}. \tag{A.5}$$

A.2 Boltzmann equations for cavitating two-phase flow

Based on the application of the gas kinetic theory, the Boltzmann equation that describes the velocity distribution function. f_k of the k phase in the cavitating two-phase flow is as follows (X. L. Tang and J. Wu [18]):

$$\frac{\partial f_k}{\partial t}+\frac{\partial f_k}{\partial\mathbf{R}_k}\frac{d\mathbf{R}_k}{dt}+\frac{\partial f_k}{\partial c_k}\frac{dc_k}{dt}+\frac{\partial f_k}{\partial\theta_k}\frac{d\theta_k}{dt}+\frac{\partial f_k}{\partial r_k}\frac{dr_k}{dt}=\left(\frac{\partial f_k}{\partial t}\right)_{kc}+\left(\frac{\partial f_k}{\partial t}\right)_{k'c}, \tag{A.6}$$

where the subscripts $k=l$ and ca represent the liquid phase and cavity phase in cavitating flow respectively; dr_k/dt is the rate of radius change of micro cavities in the cavity phase. And

$$\frac{d\mathbf{R}_k}{dt}=\mathbf{c}_k,\quad \frac{d\mathbf{c}_k}{dt}=\frac{\mathbf{F}_k}{m_k},$$

where $\mathbf{F}_k$ is the mass force of the k phase fluid, and m_k is the cavity mass or liquid mass of the k phase flow. If $k'=l,ca$, and $k'\neq k$; then $(\partial f_k/\partial t)_{kc}$ and $(\partial f_k/\partial t)_{k'c}$ are the terms for the collision of vapor molecules or liquid molecules in the same phase and between vapor molecules and liquid molecules of two different phases. The subscript c denotes the collision effect.

For cavitating two-phase flow, it is assumed that the temperature of the cavity and liquid does not change, so that the fourth term on the left-hand side of Eq. (A.6) is ignored. But the collision between liquid molecules and vapor molecules can not be neglected; thus the right-hand side of Eq. (A.6) is not equal to zero.

Integrate Eq. (A.6) after multiplying its two sides by any variable Φ_k, and the following integrated equation can be obtained:

$$\begin{aligned}&\int\Phi_k\frac{\partial f_k}{\partial t}d\mathbf{c}_k+\int\Phi_k\mathbf{c}_k\cdot\frac{\partial f_k}{\partial\mathbf{R}_k}d\mathbf{c}_k+\int\Phi_k\frac{\mathbf{F}_k}{m_k}\cdot\frac{\partial f_k}{\partial\mathbf{c}_k}d\mathbf{c}_k+\int\Phi_k\frac{\partial f_k}{\partial r_k}\frac{dr_k}{dt}d\mathbf{c}_k\\&=\int\Phi_k\Big(\frac{\partial f_k}{\partial t}\Big)_{kc}d\mathbf{c}_k+\int\Phi_k\Big(\frac{\partial f_k}{\partial t}\Big)_{k'c}d\mathbf{c}_k.\end{aligned}\tag{A.7}$$

Because variables t, $\mathbf{c}_k$ and $\mathbf{R}_k$ are independent of each other, the four terms on the left-hand side of Eq. (A.7) can be expressed as (Chen [19]):

$$\int\Phi_\kappa\frac{\partial f_k}{\partial t}d\mathbf{c}_k=\frac{\partial}{\partial t}\int\Phi_\kappa f_k d\mathbf{c}_k=\frac{\partial}{\partial t}\big(n_k\langle\Phi_\kappa\rangle\big),\tag{A.8a}$$

$$\int\Phi_\kappa\mathbf{c}_k\cdot\frac{\partial f_k}{\partial\mathbf{R}_k}d\mathbf{c}_k=\frac{\partial}{\partial R_k}\cdot\int\Phi_\kappa\mathbf{c}_k f_k d\mathbf{c}_k=\frac{\partial}{\partial R_k}\cdot\Big(n_k\big\langle\Phi_\kappa\mathbf{c}_k\big\rangle\Big),\tag{A.8b}$$

$$\int\Phi_\kappa\frac{\mathbf{F}_k}{m_k}\cdot\frac{\partial f_k}{\partial\mathbf{c}_k}d\mathbf{c}_k=\int\frac{F_k}{m_k}\cdot\Big[\frac{\partial(\Phi_\kappa f_k)}{\partial\mathbf{c}_k}-f_k\frac{\partial\Phi_\kappa}{\partial\mathbf{c}_k}\Big]d\mathbf{c}_k=-\frac{\mathbf{F}_k}{m_k}\cdot\Big(n_k\big\langle\frac{\partial\Phi_\kappa}{\partial\mathbf{c}_k}\big\rangle\Big),\tag{A.8c}$$

$$\int\Phi_k\frac{\partial f_k}{\partial r_k}\frac{dr_k}{dt}d\mathbf{c}_k=\frac{r_{k0}-r_k}{\sigma^2}\frac{dr_k}{dt}\int\Phi_k f_k d\mathbf{c}_k=\frac{r_{k0}-r_k}{\sigma^2}\frac{dr_k}{dt}\big(n_k\langle\Phi_k\rangle\big),\tag{A.8d}$$

where n_k is the cavity or liquid molecule number in a unit volume. Eq. (A.8d) can be obtained in the following Eqs. (A.9) to (A.11).

The transportation equations of cavity- and liquid-phase macro variables can be expressed as following.

The distribution function f_k is given in the following form:

$$f_k(\mathbf{R},\mathbf{c},\theta,r,t)=K(\mathbf{R},\mathbf{c},\theta,t)\Big(\frac{1}{2\pi\sigma^2}\Big)^{\frac{1}{2}}\exp\Big(-\frac{(r_k-r_{k0})^2}{2\sigma^2}\Big),\tag{A.9}$$

where r_{k0} is the initial value of r_k.

With a series of deduction, macro-variables' (statistical averaged variables) transportation equation can be finally written as follows:

$$\frac{\partial}{\partial t}\left(n_k\langle\Phi\rangle\right)+\frac{\partial}{\partial x_{ki}}\left(n_k\langle\Phi\mathbf{c}_{ki}\rangle\right)-\frac{1}{m_k}\mathbf{F}_{ki}\frac{\partial}{\partial\mathbf{c}_{ki}}\left(n_k\langle\Phi\rangle\right)+\frac{r_{k0}-r_k}{\sigma^2}\frac{dr_k}{dt}\left(n_k\langle\Phi_k\rangle\right)$$
$$=\int\Phi\Big[\Big(\frac{\partial f_k}{\partial t}\Big)_{kc}+\Big(\frac{\partial f_k}{\partial t}\Big)_{k'c}\Big]d^3\mathbf{c}_{kj}. \tag{A.10}$$

Rayleigh gave the solution of the spherical micro cavity based on the Rayleigh equation in cavity dynamics (Brennen [20]), and Plesset obtained the modified solution, which is

$$\frac{dr_k}{dt}=\pm\sqrt{\frac{2|p-p_v|}{3\rho_l}}, \tag{A.11}$$

where p_v is the vapor pressure of liquid.

A.3 Continuous equations of cavity- and liquid-phase's macro-variables

Assuming that collision causes no mass transportation between and inside the phases, and let $\Phi_k=m_k$ in transportation equation, the k-phase continuous equation can be obtained as:

$$\frac{\partial\alpha_k\rho_k}{\partial t}+\frac{\partial}{\partial x_j}(\alpha_k\rho_k\mathbf{u}_{kj})=S_k, \tag{A.12}$$

where S_k is the mass transportation caused by the variation of the cavity diameter

$$S_k=-\frac{r_{k0}-r_k}{\sigma^2}\frac{dr_k}{dt}(n_km_k)=-\frac{r_{k0}-r_k}{\sigma^2}\frac{dr_k}{dt}(\alpha_k\rho_k). \tag{A.13}$$

Introducing the cavity mass fraction f_{ca} and its relation with volume fraction α is

$$\alpha_{ca}=f_{ca}\frac{\rho}{\rho_v}, \tag{A.14}$$

where ρ_{ca} is the vapor density, and $\rho=\alpha_{ca}\rho_{ca}+\alpha_l\rho_l$ and the mass transfer expression is as follows:

$$S_k=(n4\pi)^{\frac{1}{3}}(3\alpha_k)^{\frac{2}{3}}\frac{\rho_{ca}\rho_l}{\rho}\Big[\frac{2}{3}\Big(\frac{p_v-p}{\rho_l}\Big)\Big]^{\frac{1}{2}}, \tag{A.15}$$

where n is the cavity number if a unit volume and is determined by the initial conditions of cavity. For example, the initial cavity phase mass fraction $f_{ca}=1-77mg/m^3$ and $r_0=3-10\mu m$ and then can get n, the cavity number in one unit volume.

A.4 Momentum equations of cavity- and liquid-phase's macro-variables

When $\Phi = m_k c_{ki}$ in the transportation equation, k-phase's momentum equation can be obtained. Since $\rho_k\langle c_{ki}c_{kj}\rangle = \rho_k\langle(\mathbf{u}_{ki}+c'_{ki})(\mathbf{u}_{kj}+c'_{kj})\rangle = \rho_k\mathbf{u}_{ki}\mathbf{u}_{kj}+T_{kij}$, $F_{ki} = m_k g_{ki}$, we can obtain,

$$\frac{\partial}{\partial t}\left(\rho_k\langle c_{kj}\rangle\right)+\frac{\partial}{\partial x_{ki}}\left(\rho_k\langle c_{ki}c_{kj}\rangle\right)-n_k F_{ki}\frac{\partial}{\partial c_{ki}}\langle c_{kj}\rangle = \int m_k c_{kj}\left[\left(\frac{\partial f_k}{\partial t}\right)_{kc}+\left(\frac{\partial f_k}{\partial t}\right)_{k'c}\right]d^3c_{kj}, \quad \text{(A.16)}$$

where F_{ki} is the k-phase mass force. The k-phase stress tensor is

$$T_{kij} = \langle c'_{ki}c'_{kj}\rangle = \int (c_{ki}-\mathbf{u}_{ki})(c_{kj}-\mathbf{u}_{kj})f_k d^3c_{kj} = p_k\delta_{ij}-\tau_{kij}. \quad \text{(A.17)}$$

In above equation, the k-phase's partial pressure is $p_k = (T_{k11}T_{k22}+T_{k33})/3$; and τ_{kij} is viscosity stress tensor.

Given that collision inside the phases experiences no energy losses and obeys the conversation law, the first collision term on the equation's right side in Eq. (A.16) equals zero. The second term describes the collision between cavity phase and liquid phase, that is, the interaction force between phases. The formula to expreee the interaction force can be given as:

$$F = \int m_k c_{kj}\left(\frac{\partial f_k}{\partial t}\right)_{k'c} d^3c_{kj} = \frac{\rho_k}{\tau_{rca}}(\mathbf{u}_{caj}-\mathbf{u}_{lj}), \quad \text{(A.18)}$$

where

$$\tau_{rca} = \frac{d_{ca}^2\rho_{ca}}{18\mu_l}\left(1+\frac{Re_{ca}^{\frac{2}{3}}}{6}\right)^{-1}, \quad Re_{ca} = |\mathbf{u}_{ca}-\mathbf{u}_l|\frac{d_{ca}}{\nu_l}, \quad \text{(A.19)}$$

where d_{ca} is diameter of cavity in liquid, which is determined by the cavity phase volume fraction and the initiate number n in one fraction volume of the phase.

Let α_l and α_{ca} be the volume fractions of the liquid and cavity phases respectively, and $\alpha_{ca}+\alpha_l = 1$. The governing equations (continuity and the momentum equations) for the liquid-phase are

$$\frac{\partial\alpha_l\rho_l}{\partial t}+\frac{\partial}{\partial x_j}(\alpha_l\rho_l\mathbf{u}_{lj}) = S_l, \quad \text{(A.20a)}$$

$$\frac{\partial(\alpha_l\rho_l\mathbf{u}_{li})}{\partial t}+\frac{\partial}{\partial x_j}(\alpha_l\rho_l\mathbf{u}_{li}\mathbf{u}_{lj}) = \alpha_l\rho_l g_{li}-\frac{\partial(\alpha_l p)}{\partial x_i}+\alpha_l\frac{\partial\tau_{lij}}{\partial x_j} + \frac{\alpha_l\rho_l}{\tau_{rca}}\left(\mathbf{u}_{cai}-\mathbf{u}_{li}\right)+\mathbf{u}_{li}S_l, \quad \text{(A.20b)}$$

where $\mathbf{u}$ is the mean velocity in the liquid phase or cavity phase from a macroscopic view.

Appendix B: The $k-\varepsilon-k_{ca}$ turbulence model of liquid-cavity two-phase flows

The basic equations of two phase turbulent flows have been developed by Ishii [21], and further developed on the area of gas particle two phase flows by Zhou [22]. The $k-\varepsilon-k_{ca}$ turbulence model is proposed in this particular cavity-liquid two phase flow in the present simulation. This model is similar to the turbulence model in liquid particle flow proposed by Wu [23].

The $k-\varepsilon-k_{ca}$ turbulence model of two-phase flows has the isotropic characteristics and may be applied at the conditions of small circulation flows and the flows with small buoyancy forces. This model is actually the combination between the standard $k-\varepsilon$ turbulence model for liquid phase and the k_{ca} turbulence model for cavity phase, in which the Boussinesq expressions are used to indicate the second order correlation terms in transporting equations.

The turbulence model for liquid phase in the $k-\varepsilon-k_{ca}$ turbulence model can be obtained from the basic equation of two-phase turbulent flow equations reported from references [21–23]. By using the Boussinesq expressions, the following correlation terms can be simplified in the following equations:

$$-\overline{\mathbf{u}'_i\mathbf{u}'_j}=\nu_T\left(\frac{\partial \mathbf{u}_j}{\partial x_i}+\frac{\partial \mathbf{u}_i}{\partial x_j}\right)+\frac{2}{3}k\delta_{ij}, \qquad -\overline{\rho\mathbf{u}'_k\mathbf{u}'_i\mathbf{u}'_j}=\frac{\mu_e}{\sigma_k}\cdot\frac{\partial k}{\partial x_k},$$

$$D_{\varepsilon,ij}=\frac{\partial}{\partial x_k}\left(\frac{\mu_e}{\sigma_\varepsilon}\cdot\frac{\partial \varepsilon}{\partial x_k}\right), \qquad -\overline{n'_{ca}\mathbf{u}'_{cai}}=\frac{\nu_{ca}}{\sigma_{pa}}\cdot\frac{\partial n_{ca}}{\partial x_i},$$

$$-\overline{n'_{ca}\mathbf{u}'_{caj}}=\frac{\nu_{ca}}{\sigma_{ca}}\cdot\frac{\partial n_{ca}}{\partial x_j}, \qquad -\overline{n'_{ca}\mathbf{u}'_{cak}}=\frac{\nu_{ca}}{\sigma_{ca}}\cdot\frac{\partial n_{ca}}{\partial x_k},$$

where $\sigma_k=1.0$ and $\sigma_{ca}=1.5$.

The continuity equations and the momentum equations of liquid phase then can be deduced in this turbulence model:

$$\frac{\partial \rho}{\partial t}+\frac{\partial}{\partial x_j}(\rho\mathbf{u}_j)=S=-\sum n_{ca}\dot{m}_{ca}, \tag{B.1a}$$

$$\frac{\partial}{\partial t}(\rho\mathbf{u}_i)+\frac{\partial}{\partial x_j}(\rho\mathbf{u}_j\mathbf{u}_i)=-\frac{\partial P}{\partial x_i}+\frac{\partial}{\partial x_j}\left[\mu_e\left(\frac{\partial \mathbf{u}_i}{\partial x_j}+\frac{\partial \mathbf{u}_j}{\partial x_i}\right)\right]+\sum\frac{n_{ca}m_{ca}}{\tau_{rca}}(\mathbf{u}_{cai}-\mathbf{u}_i)$$
$$+\sum\frac{m_{ca}}{\tau_{rca}}\left(\frac{\nu_{ca}}{\sigma_{ca}}\cdot\frac{\partial n_{ca}}{\partial x_i}\right). \tag{B.1b}$$

And the turbulent kinetic energy k equation and the turbulent energy dissipation rate ε equation for liquid phase are as follows:

$$\frac{\partial}{\partial t}(\rho k)+\frac{\partial}{\partial x_j}(\rho\mathbf{u}_j k)=\frac{\partial}{\partial x_j}\left(\frac{\mu_e}{\sigma_k}\cdot\frac{\partial k}{\partial x_j}\right)+G_k+G_p+G_R-\rho\varepsilon, \tag{B.2a}$$

$$\frac{\partial}{\partial t}(\rho\varepsilon)+\frac{\partial}{\partial x_j}(\rho\mathbf{u}_j\varepsilon)=\frac{\partial}{\partial x_j}\Big(\frac{\mu_e}{\sigma_\varepsilon}\cdot\frac{\partial\varepsilon}{\partial x_j}\Big)+\frac{\varepsilon}{k}\big[C_{\varepsilon I}(G_k+G_p)-C_{\varepsilon 2}\rho\varepsilon\big], \tag{B.2b}$$

where

$$\mu_e=\mu+\mu_T, \qquad \mu_T=C_\mu\rho k^2/\varepsilon,$$
$$G_k=\mu_T\Big(\frac{\partial\mathbf{u}_i}{\partial x_j}+\frac{\partial\mathbf{u}_j}{\partial x_i}\Big)\frac{\partial\mathbf{u}_i}{\partial x_j}, \qquad G_{ca}=-\sum\frac{n_{ca}m_{ca}}{\tau_{rca}}\big[2(k-C_{ca}^k\sqrt{kk_{ca}})\big],$$

where $C_\mu=0.09$, $\sigma_k=1.0$, $\sigma_{ca}=1.3$, $C_{\varepsilon 1}=1.44$ and $C_{\varepsilon 2}=1.9$.

By using the Boussinesq expressions, the following correlation terms of cavity phase can be simplified in the following equations:

$$-\overline{\mathbf{u}'_{cai}\mathbf{u}'_{caj}}=v_{ca}\Big(\frac{\partial\mathbf{u}_{cai}}{\partial x_j}+\frac{\partial\mathbf{u}_{caj}}{\partial x_i}\Big), \qquad -\overline{\mathbf{u}'_{cak}\mathbf{u}'_{cai}}=v_{ca}\Big(\frac{\partial\mathbf{u}_{cak}}{\partial x_i}+\frac{\partial\mathbf{u}_{cai}}{\partial x_k}\Big),$$
$$-\overline{n'_{ca}\mathbf{u}'_{cai}}=\frac{v_{ca}}{\sigma_{ca}}\cdot\frac{\partial n_{ca}}{\partial x_i}, \qquad -\overline{n'_{ca}\mathbf{u}'_{caj}}=\frac{v_{ca}}{\sigma_{ca}}\cdot\frac{\partial n_{ca}}{\partial x_j},$$
$$-\overline{n'_{ca}\mathbf{u}'_{ck}}=\frac{v_{ca}}{\sigma_{ca}}\cdot\frac{\partial n_{ca}}{\partial x_k}, \qquad -\overline{\mathbf{u}'_{cak}\mathbf{u}'_{cai}\mathbf{u}'_{caj}}=\frac{v_{ca}}{\sigma_{ca}}\cdot\frac{\partial k_{ca}}{\partial x_k},$$

where $\sigma_{ca}=1.5$ and $C_{ca}^k=0.11$.

The continuity equations and the momentum equations of cavity phase then can be deduced in this turbulence model:

$$\frac{\partial n_{ca}}{\partial t}+\frac{\partial}{\partial x_j}(n_{ca}\mathbf{u}_{caj})=\frac{\partial}{\partial x_j}\Big(\frac{v_{ca}}{\sigma_{ca}}\cdot\frac{\partial n_{ca}}{\partial x_j}\Big), \tag{B.3a}$$

$$\frac{\partial}{\partial t}(n_{ca}\mathbf{u}_{cai})+\frac{\partial}{\partial x_j}(n_{ca}\mathbf{u}_{caj}\mathbf{u}_{cai})=\frac{\partial}{\partial x_j}\Big[n_{ca}v_{ca}\Big(\frac{\partial\mathbf{u}_{cai}}{\partial x_j}+\frac{\partial\mathbf{u}_{caj}}{\partial x_i}\Big)\Big]+\frac{m_{ca}+\dot{m}_{ca}\tau_{rca}}{m_{ca}\tau_{rca}}n_{ca}(\mathbf{u}_i-\mathbf{u}_{cai})$$
$$+\frac{\partial}{\partial x_j}\Big(\mathbf{u}_{cj}\frac{v_{ca}}{\sigma_{ca}}\cdot\frac{\partial n_{ca}}{\partial x_i}+\mathbf{u}_{cai}\frac{v_{ca}}{\sigma_{ca}}\cdot\frac{\partial n_{ca}}{\partial x_j}\Big)-\frac{m_{ca}+\dot{m}_{ca}\tau_{rca}}{m_{ca}\tau_{rcca}}\cdot\frac{v_{ca}}{\sigma_{ca}}\cdot\frac{\partial n_{ca}}{\partial x_i}+\frac{\partial}{\partial t}\Big(\frac{v_{ca}}{\sigma_{ca}}\cdot\frac{\partial n_{ca}}{\partial x_i}\Big). \tag{B.3b}$$

And the turbulent kinetic energy k_{ca} transporting equation and for cavity phase is as follows:

$$\frac{\partial}{\partial t}(n_{ca}k_{ca})+\frac{\partial}{\partial x_j}(n_{ca}\mathbf{u}_{caj}k_{ca})=\frac{\partial}{\partial x_j}\Big(n_{ca}\frac{v_{ca}}{\sigma_{ca}}\cdot\frac{\partial k_{ca}}{\partial x_j}\Big)+G_{kca}+G_{pca}-n_{ca}\varepsilon_{ca}, \tag{B.4}$$

where

$$G_{kca}=n_{ca}v_{ca}\Big(\frac{\partial\mathbf{u}_{caj}}{\partial x_j}+\frac{\partial\mathbf{u}_{cai}}{\partial x_j}\Big)\frac{\partial\mathbf{u}_{cai}}{\partial x_j}, \quad G_{pca}=\frac{v_{ca}}{\sigma_{ca}}\Big(\frac{\partial n_{ca}}{\partial x_i}\cdot\frac{\partial\mathbf{u}_{cai}}{\partial x_j}\Big),$$
$$\varepsilon_{ca}=-\frac{m_{ca}+\dot{m}_{ca}\tau_{rca}}{m_{ca}\tau_{rca}}\Big[2(C_{ca}^k\sqrt{kk_{ca}}-k_{ca})+\frac{\mathbf{u}_i}{n_{ca}}\cdot\frac{v_{ca}}{\sigma_{ca}}\cdot\frac{\partial n_{ca}}{\partial x_i}\Big],$$

where $\sigma_{ca}=1.5$ and $C_{ca}^{k}=0.11$.

Eqs. (B.1) to (B.4) form the isotropic $k-\varepsilon-k_{ca}$ turbulence model of two-phase flows by expression in the form of cavity number instead of the form of cavity phase volume fraction. This model is similar to the equations of two fluid flow model for the silt laden flow by Tang and Wu [18] and Wu [23].

From Eqs. (B.1a), (B.1b), (B.3a) and (B.3b) can form the basic equations of the mixed flow model for the liquid cavity flow [19]. The mixed flow model for the liquid cavity flow has been used for the cavitating flow computation now [12] and [24], in which there is the mass transfer term to be considered. And in two fluid model both the momentum transfer term and the mass transfer term are considered. For example, the widely used software of CFD, Fluent and CFX have adopted the mixed model to calculate the cavitating flows in Engineering application.

The advantage using the cavity number instead of the cavity phase volume fraction is explained as follows.

In two-phase flow, the calculation of the density can be expressed as

$$\rho_m=\rho_l+\rho_{ca}=\rho_l+n_{ca}m_{ca}=\rho_l+\bar{\rho}_{ca}n_{ca}\frac{\pi d_{ca}^3}{6}, \tag{B.5}$$

where ρ_m is the density of mixture, ρ_l is the fluid bulk density, ρ_{ca} is the cavity bulk density, $\bar{\rho}_{ca}$ is the cavity material density, and n_{ca} is the cavity number in the unit volume.

The volume fractions of the fluid phase C_l and the cavity phase C_{ca} are defined as:

$$C_{ca}=\frac{\rho_{ca}}{\bar{\rho}_{ca}}, \tag{B.6a}$$

$$C_l=\frac{\rho_l}{\bar{\rho}_l}=1-C_{ca}=1-\frac{\rho_{ca}}{\bar{\rho}_{ca}}. \tag{B.6b}$$

From the relations between deferent density determinations of multiphase flows, the forgoing governing equations (B.3a)-(B.4) can be also transformed into the equation expressed in the volume fraction, like in most application of the equations in the mixed model.

Although, some researchers through their experiments observed that the cavity clouds had a concentrated vorticity region at the clouds center and contained clusters of many small cavitation bubbles (many cavities). This phenomenon prediction would be beyond the ability of the present CFD cavitating simulations of the mixture model based on the homogeneous flow treatment [25]. In the mixture model, it is assumed that the cavity number in the unit volume of mixture is not changed in the cavity phase transfer, and the cavity volume change is caused only by the cavity diameter variation from the solution of the Rayleigh-Plesset equation. The foregoing Eqs. (B.3a)-(B.4) have the possibility to predict the variations both of cavity diameter and cavity number in a unit volume. Therefore, the model developed in present study can predict the cavitation clouds.

Nomenclature

$\mathbf{c}$	velocity of molecules of the liquid phase or cavity phase
$\mathbf{c}'$	relative velocity of molecules to the mean macroscopic velocity
d	cavity diameter
E, k	constants
$\mathbf{F}_k$	mass force of the k phase fluid
f	velocity distribution function
g	gravity acceleration
k	turbulent kinetic energy
m	the cavity mass or liquid mass
N	micro molecule number
n	bubble or micro molecules' number density, normal
p	pressure
S	mass transfer term
Re	Reynolds number
$\mathbf{R}$	geometrical space
$\mathbf{R}_k$	vector radius of micro cavity
r	radius space of molecules
t	time
$\mathbf{u}$	mean velocity in the liquid phase or cavity phase
u_j	velocity component
u, v, w	velocity components along X, Y, Z in sump
X, Y, Z	ordinates in sump
x_j	Cartesian ordinate
α	volume fraction (VF)
ε	turbulent kinetic energy dispassion rate
μ	viscosity
ν	kinetic viscosity
ρ	density
τ	stress
θ	temperature
Φ	a physical variable
σ	standards difference
$\langle\rangle$	statistical mean value
ca	cavity phase
l	liquid phase
p	point near wall

Acknowledgments

This research work was funded by the Chinese National Foundation of Natural Science

(Nos. 51076077, 51176168, 51249003 and 51076144). This work is also supported by Science Foundation of Zhejiang Sci-Tech University (ZSTU) under Grant No. 11130032241201.

References

[1] H. YAMAGUCHI AND H. KATO, *On application of nonlinear cavity flow theory to thick foil sections*, Proc. Conf. Cavitation, Inst. Mech. Eng., Edinburgh, Scotland, 1983.

[2] W. H. BREWER AND S. A. KINNAS, *Experimental and computational investigation of sheet cavitation on a hydrofoil*, in FED Cavitation and Multiphase Flow, ASME FED 210, Y. Matsumoto and J. Katz, Eds., American Soc. of Mechanical Engineers, New York, USA, 1995, pp. 1–15.

[3] C. PELLONE AND J. M. PEALLAT, *Non-linear analysis of three-dimensional partially cavitating hydrofoil*, in Proc. of the International Symposium on Cavitation, B. D. des Carenes, Ed., Deauville, France, May 2-5, 1995, EPFL, Lausanne, Switzerland (1995), pp. 63–67.

[4] D. F. DE LANGE AND G. J. DE BRUIN, *Sheet cavitation and cloud cavitation re-entrant jet and three-dimensionality*, Appl. Scic Res., 58 (1998), pp. 91–114.

[5] A. KUBOTA, H. KATO AND H. YAMAGUCH, *A new modeling of cavitating flows, a numerical study of unsteady cavitation on a hydrofoil section*, J. Fluid Mech., 240 (1992), pp. 59–96.

[6] C. C. S. SONG, J. HE, F. ZHOU AND G. WANG, Numerical Simulation of Cavitating and Non-cavitating Flows over a Hydrofoil, SAFL project report No. 402, St. Anthony Falls Laboratory, University of Minnesota, Minneapolis, USA, 1997.

[7] R. E. A. ARNDT, M. KJELDSEN, C. C. S. SONG AND A. KELLER, *Analysis of cavitation wake flows*, in Proc. of the 21st IAHR Symposium on Hydraulic Machinery and Systems, F. Avellan, G. Ciocan and S. Kvicinsky, Eds., Lausanne, Switzerland, September 9-12, Inter. Assoc. on Hydraulic Research, Section on Hydraulic Machinery and System, Lausanne, Switzerland (2002), Paper No. A91-XOBKLURZ.

[8] Q. QIN, C. S. S. SONG AND R. E. ARNDT, *Numerical study of unsteady turbulent wake behind a cavitating hydrofoil*, in Proc. of 5th International Symposium on Cavitation, CAV2003, Y. Matsumoto and Y. Tsujimoto Eds. Osaka, Japan, November 1-4, 2003, Osaka University, Osaka, Japan, Paper No. EM.003 (2003).

[9] Y. CHEN, Y. AND D. HEISTER, *A numerical treatment for attached cavitation*, J. Fluids Eng., 116 (1994), pp. 613–618.

[10] M. DESHPANDE, J. FENG AND C. L. MERKLE, *Numerical modeling of the thermodynamic effects of cavitation*, J. Fluids Eng., 119 (1997), pp. , 420–426.

[11] Y. VENTIKOS AND G. TZABIRAS, *A numerical method for the simulation of steady and unsteady cavitating flows*, Computer Fluids, 29 (2000), pp. 63–88.

[12] A. K. SINGHAL, N. VAIDYA AND A. D. LEONARD, *Multi-dimensional simulation of cavitating flows using a PDF model for phase change*, In: Proceeding of ASME Fluids Engineering Division Summer Meeting, Vancouver, 4 (1997), pp. 1–8.

[13] C. L. MERKLE, J. Z. FENG AND P. E. BUELOW, *Computational modeling of the dynamics of sheet cavitation*, in Proc. Third Int. Symposium on Cavitation, J.-M. Michel and H. Kato Eds., April 7-10, 1998, Grenoble, France, EPFL, Lausanne, Switzerland (1998), pp. 307–311.

[14] R. F. KUNZA, D. A. BOGERA, D. R. STINEBRINGA, T. S. CHYCZEWSKIA, J. W. LINDAUA, H. J. GIBELINGA, S. VENKATESWARANB AND T. R. GOVINDANC, *A preconditioned Navier-Stokes method for two-phase flows with application to cavitation prediction*, Comput Fluids, 29 (2000), pp. 849–875.

[15] I. SENOCAK AND W. SHYY, *A pressure-based method for turbulent cavitating flow computation*, J. Comput. Phys., 176 (2002), pp. 363–383.
[16] R. RIEGER, Mehrdimensionale Berechnung zweiphasiger Stroemungen, PhD-Thesis, Technical University Graz, Graz, Austria, 1992.
[17] H. A. GROGGER AND A. ALAJBEGOVIC, *Calculation of the cavitation flow in venturi geometries using two fluid model*, in Proc. of ASME Fluids Eng. Division Summer Meeting, C. J. Freitas Ed., Washington D. C., USA, June 22-25, 1998, American Soc. of Mechanical Engineers, New York, USA (1998), Paper No. FEDSM98-5295.
[18] X. L. TANG AND J. WU, *An improved les on dense particle-liquid turbulent flows using integrated Boltzmann equations*, Can. J. Chem. Eng., 85 (2007), pp. 137–150.
[19] X. CHEN, Dynamic Theory and Its Application in Thermophysics and Fluid Flow, Tsinghua University Press, Beijing, China, 1996, pp. 58–66, 67–74 (in Chinese).
[20] C. E. BRENNEN, Cavitation and Bubble Dynamics, Oxford University Press, New York, USA, 1995, Chapter 2, pp. 1–10.
[21] M. ISHII, Thermo-Fluid Dynamic Theory of Two-Phase Flow, 1975, Eyrolles, Paris.
[22] L. X. ZHOU, Theory of Gas-Particle Two-Phase Flow and Combustion and Its Numerical Simulation, Publisher of Sciences in China, 1994.
[23] Y. L. WU, Numerical Simulation of Liquid-Particle Two-Phase Flows Through Hydraulic Machinery by Two-Fluid Model (Chapter 3), Abrasive Erosion and Corrosion of Hydraulic Machinery, Editors: C. G. Duan and V. Y. Karelin, Imperiral College Press, London, 2002.
[24] A. K. SINGHAL, H. Y. LI, M. M. ATHAVALE AND Y. JIANG, *Mathematical basis and validation of the full cavitation model*, in Proc. of ASME FEDSM'01, 2001 ASME Fluids Eng. Division Summer Meeting, J. Katz, Ed., New Orleans, Louisiana, May 29-June 1, 2001, American Soc. of Mechanical Engineers, New York, USA, 1997, Paper No. FEDSM2001-18015.
[25] B. JI, X. W. LUO, Y. L. WU, X. X. PENG AND Y. L. DUAN, *Numerical analysis of unsteady cavitating turbulent flow and shedding horse-shoe vortex structure around a twisted hydrofoil*, Submitted to International Journal of Multiphase Flow, 2012, (accepted).